Direct water-assisted laser desorption/ionization mass spectrometry lipidomic analysis and classification of formalin-fixed paraffin-embedded sarcoma tissues without dewaxing

Nina Ogrinc, Pierre-Damien Caux, Yves-Marie Robin, Emmanuel Bouchaert, Benoit Fatou, Michael Ziskind, Cristian Focsa, Delphine Bertin, Dominique Tierny, Zoltan Takats, et al.

Clinical Chemistry 67:11
1513–1523 (2021)

Direct Water-Assisted Laser Desorption/Ionization Mass Spectrometry Lipidomic Analysis and Classification of Formalin-Fixed Paraffin-Embedded Sarcoma Tissues without Dewaxing

Nina Ogrinc,[a] Pierre-Damien Caux,[a] Yves-Marie Robin,[a,b] Emmanuel Bouchaert,[a,c] Benoit Fatou,[a] Michael Ziskind,[d] Cristian Focsa,[d] Delphine Bertin,[b] Dominique Tierny,[a,c] Zoltan Takats,[a] Michel Salzet,[a,e] and Isabelle Fournier[a,e,*]

BACKGROUND: Formalin-fixed paraffin-embedded (FFPE) tissue has been the gold standard for routine pathology for general and cancer postoperative diagnostics. Despite robust histopathology, immunohistochemistry, and molecular methods, accurate diagnosis remains difficult for certain cases. Overall, the entire process can be time consuming, labor intensive, and does not reach over 90% diagnostic sensitivity and specificity. There is a growing need in onco-pathology for adjunct novel rapid, accurate, reliable, diagnostically sensitive, and specific methods for high-throughput biomolecular identification. Lipids have long been considered only as building blocks of cell membranes or signaling molecules, but have recently been introduced as central players in cancer. Due to sample processing, which limits their detection, lipid analysis directly from unprocessed FFPE tissues has never been reported.

METHODS: We present a proof-of-concept with direct analysis of tissue-lipidomic signatures from FFPE tissues without dewaxing and minimal sample preparation using water-assisted laser desorption ionization mass spectrometry and deep-learning.

RESULTS: On a cohort of difficult canine and human sarcoma cases, classification for canine sarcoma subtyping was possible with 99.1% accuracy using "5-fold" and 98.5% using "leave-one-patient out," and 91.2% accuracy for human sarcoma using 5-fold and 73.8% using leave-one-patient out. The developed classification model enabled stratification of blind samples in <5 min and showed >95% probability for discriminating 2 human sarcoma blind samples.

CONCLUSION: It is possible to create a rapid diagnostic platform to screen clinical FFPE tissues with minimal sample preparation for molecular pathology.

Introduction

Fast and accurate tumor diagnosis is critical in clinical decision-making for optimal patient care. The common preservation technique is the creation of formalin-fixed paraffin-embedded (FFPE) tissue specimens. FFPE blocks are extremely stable, enable indefinite storage, and offer well preserved tissue morphology for postoperative histological assessment. Despite the integration of multimodal histological and molecular exams, cancer diagnostics remains labor intensive, difficult, and in need of ancillary techniques (1, 2).

Mass spectrometry imaging has quickly emerged as a tool to study molecular biochemistry in situ. Particularly, matrix-assisted laser desorption ionization (MALDI) and desorption electrospray ionization (DESI), have growing interest as molecular histology tools. In oncology, these techniques have been shown useful for diagnostics, prognostics, cancer classification, patient stratification, and to study tumor microenvironment (3–5). However, to promote the integration of mass spectrometry techniques into postoperative diagnostics, it is paramount to apply them to FFPE samples.

[a]University of Lille, Inserm, CHU Lille, U1192 - Protéomique Réponse Inflammatoire Spectrométrie de Masse–PRISM, Lille, France; [b]Unité de Pathologie Morphologique et Moléculaire, Centre Oscar Lambret, Lille, France; [c]OCR (Oncovet Clinical Research), Parc Eurasante Lille Metropole, Loos, France; [d]University of Lille, CNRS, UMR 8523, PhLAM–Physique des Lasers, Atomes et Molécules, Lille, France; [e]Institut Universitaire de France (IUF), Paris, France

*Address correspondence to this author at: Laboratoire Protéomique, Réponse Inflammatoire et Spectrométrie de Masse (PRISM)–Inserm U1192–Université de Lille, Bât SN3, 1er étage, Cité Scientifique, F-59655 Villeneuve d'Ascq Cedex, France. Fax +33 (0)3 20 43 40 54; e-mail isabelle.fournier@univ-lille.fr.

Received February 17, 2021; accepted July 26, 2021.
DOI: 10.1093/clinchem/hvab160

Molecular analysis from FFPE tissues is challenging due to paraformaldehyde reacting with free amine groups, giving rise to Schiff-bases and further crosslinking by the formation of methylene bridges (i.e., proteins, DNA, RNA) (6). Strategies have been proposed to unlock and image proteins by MALDI–MSI (7, 8) and have given rise to comprehensive, highly reproducible bottom-up proteomic or glycan approaches (9, 10). These protocols are not only time consuming but also require expertise in sample preparation, analysis, and data processing (7–9, 11).

Direct mass spectrometric analysis of lipids from tissues has begun to gain importance in cancer research (12). Lipids are now recognized as a central contributors to the pathophysiological mechanisms (13) and changes in cell phenotypes, and lipid imaging has been proposed as an alternative to histopathology (3, 14). Unfortunately, the entire FFPE process compromises analysis of several lipid classes either due to formaldehyde fixation (FF) (15, 16) or the requirement to deparaffinize and rehydrate the samples before analysis.

Several studies have evaluated lipids and metabolites from FFPE tissues. Some metabolites, such as galactose-1-phosphate, were found using MALDI–MSI after deparaffinization and rehydration (17, 18). The following studies, however, confirmed loss of metabolite and lipid species by deparaffinization (19) and rehydration, with 80 common metabolites detected in FFPE, FF, and fresh-frozen kidney tissues (20). Even with well-thought processing by a combination of solvents and heating the paraffin (21), the detection of metabolites was 40% lower in FFPE compared to fresh-frozen material. Recently, unfixed, FF and FFPE samples using the same protocol were compared (22) and showed the recovery of ∼40–50% lipids and metabolites.

Our experimental data indicate it is possible to detect over hundred lipid species from FFPE rat brain and sarcoma tissues without deparaffinization and minimal sample preparation using water-assisted laser desorption ionization mass spectrometry (WALDI–MS) by the SpiderMass technology (23–25). These lipid species showed histopathological specificity in difficult canine and human sarcoma subtypes and were used to build classification models that enabled stratification of blind samples in <5 min.

Materials and Methods

TISSUE SAMPLES AND STUDY DESIGN

Two-year old FFPE tissue blocks of Adult Wistar male rat brain (225–250 g, 7–8 weeks of age) were collected and sectioned at 8 µm with a microtome (Leica Biosystems, Germany). Canine patient FFPE samples fixed in 10% formol solution were collected after signed owner consent. The archived tissue blocks (2013–2017) were selected according to 4 different pathologies: angiosarcoma (22 patients, 45 samples), leiomyosarcoma (4 patients, 25 samples), fibrosarcoma (1 patient, 2 samples), and the malignant tumor of peripheral nerve sheaths (2 patients, 4 samples). Archived FFPE human soft tissue tumor blocks (2013–2019), fixed in 4% formol solution (QPath, VWR) from the Comprehensive Cancer Center Oscar Lambret tumor bank were retrieved after securing patient consent; leiomyomas (4 patients, 6 samples), leiomyosarcomas (9 patients, 10 samples), lipomas (8 patients, 10 samples), and liposarcomas (8 patients, 11 samples). Sample size, collection, and inclusion were dependent on the clinical availability. The first 7 µm section was hematoxylin-phloxine-saffron stained and the consecutive section was prepared for SpiderMass analysis. The veterinary pathologist (authors E.B. and D.T.) read and annotated hematoxylin-phloxine-saffron stained canine sarcoma tissues, and the board-certified pathologist (author Y.-M.R.) annotated the human sarcoma samples. For the test analysis, 2 blind samples of human sarcoma were randomly selected from the initial cohort. All experiments were approved by the local Ethics Committee (CPP Nord Ouest IV 12/10) in accordance with the French and European legislation.

SAMPLE PREPARATION

The FFPE tissues were manually sprayed with a glycerol/isopropyl alcohol (IPA) (8:2, v/v) solution in 2 successive passes using a manual sprayer (Agilent). The syringe pump (74 900 series Cole Parmer Instrument Company) was set to a 300 µL/min flow rate. The 2 successive passes were equal to 5 µL deposited on 1 cm^2 and took ∼10 s. The samples could be analyzed up to 30 min after glycerol deposition. To investigate the influence of dewaxing, several tissue sections were dewaxed in xylene for 5 min in 2 separate jars and rehydrated in ethanol baths of descending order from 90% to 70% and then 30% (5 min each). The slides were than immersed into two 10 mM ammonium bicarbonate solutions (5 min) and dried in the desiccator before glycerol deposition.

SPIDERMASS INSTRUMENT

The basic design of the instrument setup has been described in detail elsewhere (23, 24). Briefly, the prototype was equipped with a fibered tunable wavelength laser system (Radiant v.1.0.1, OPOTEK Inc., USA) and pumped by the 1.064 µm radiation delivered by a Q-switched 10 ns pulse width Nd: YAG laser (Quantel Laser, France). The infrared laser microprobe was tuned (2.94 µm) to excite the most intense vibrational band of water (O-H). A 1-m biocompatible laser fiber with 450 µm inner diameter (HP fiber, Infrared Fiber Systems, USA) was connected to the exit of the optical parametric oscillator and focused to result in 400–

500 µm beam diameter. A Tygon® tubing (Akron, USA) was used to aspirate the ablated material and was directly connected to a quadrupole-TOF mass spectrometer interface (24) (Synapt G2s or Xevo, Waters, UK). Laser energy was fixed at 4 mJ/pulse corresponding to laser fluence of 3.18 J/cm^2.

SPIDERMASS EXPERIMENTS

The laser sampling position of sarcoma samples was determined based on histopathological annotations. The samples were randomized to avoid batch effects. The acquisition was composed of 10 laser shots consecutively fired between 2–4 times with a 10 s pause. Ten laser shots result in 1 individual spectrum. The data were acquired in positive and negative sensitivity modes for rat brain tissue and positive mode for sarcoma, with 1 s scan time and 22 000 mass resolution. The mass range included *m/z* 50–2000. The acquired spectra were scaled using MassLynx software (v.4.2 SNC966, Waters Laboratory Informatics). MS/MS was performed with collision-induced dissociation with collision energy ranging between 25 and 40 V. The lipid annotations were performed manually through fragmentation spectra guidelines, and compared to LIPIDMAPS and the METLIN database (26, 27).

STATISTICAL ANALYSIS

SpiderMass raw positive ion mode data were imported into Abstract Model Builder (AMX, v.1.0 1972.0, Waters, Hungary). Classification models were built using individual spectra (mean 3 per sample) and by subjecting them to principal component analysis (PCA) and linear discriminant analysis (LDA). PCA was used to decrease the dimensionally of the data and to provide an overview of the variance in the data. LDA was used to optimize the separation between user assigned classes. The canine classification model was built using a mass range of 600–1000 *m/z* with a 0.2 binning, 1e^3 threshold intensity, applied total intensity normalization, and background subtraction. The human sarcoma model was built with the same parameters. The performance of LDA was assessed by cross-validation. Cross-validation was performed by removing a part of the cohort and building the model again. In the experiments, a "5-fold" and "leave-one-patient" out cross-validation were performed on the built models. Nonparametric one-way ANOVA (Kruskal–Wallis) followed by Dunn's test was performed to calculate significant differences between normalized intensities for discriminative ions.

BLIND TISSUE ANALYSIS

To test the efficiency of our databank, we used the Abstract Model Builder Recognition plugin of the AMX software. The same preprocessing was applied to the unclassified (test) specimens. The discriminating molecular patterns of the test specimen were extracted by means of the PCA-LDA projection matrix. The Mahalanobis distances were calculated from each previously assigned class mean. The algorithm classified the novel spectrum into the closest class, unless the distance was larger than a user defined $n \times$ standard deviation of that class. In this particular experiment, the outlier limit was set to 5 standard deviations. The other parameters set were 1e^3 TIC intensity threshold, 5 scans/spectrum, and 5 s timeout.

Results

OPTIMIZATION OF WALDI-MS FOR ANALYZING FFPE TISSUES

The first assessment was performed on a non-processed FFPE rat brain tissue section in both polarities (Fig. 1). Lipid ions were detected albeit at lower intensity (10e^3–10e^4 range, $n = 4$) than expected from fresh-frozen tissue (10e^5–10e^6 range; $n = 50$) (24). The detected species corresponded to specific fatty acids (*m/z* 200–400) and phospholipids species (*m/z* 700–900) in both polarities (Fig. 1, A and B, top section). The signals were tissue specific and were not detected in paraffin alone (Fig. 1, A and B, bottom section).

Lower ion intensities could be explained by the extremely low water content in samples, which reduced the desorption/ionization efficiency of the WALDI process. To increase the signal intensity, we deposited a glycerol matrix on top of the tissues. The glycerol O–H bond has an absorption band relatively close to the one of water, and provides important resonant excitation to generate a similar desorption/ionization process (28). Because of the high viscosity of glycerol, the tissues were uniformly sprayed with a 50% glycerol/50% IPA solution. The resulting lipid intensities increased, reaching absolute intensities up to 10e^6 (Fig. 1, A and B, middle section) in both polarities. In the negative ion mode, there was a clear mean increase of 100-fold ($n = 3$) of fatty acids, such as *m/z* 255.2 (palmitic acid), and *m/z* 281.2 (oleic acid), phosphatidic acid (PA), and phosphatidinositol (PI) lipid species *m/z* 747.5 [PA (22:6_18:0)-H]$^-$, and *m/z* 885.5 [PI (18:0_20:4)-H]$^-$ as well as a ganglioside GM 1 (18:0) at *m/z* 1544.7. In the positive ion mode, a mean 400-fold increase ($n = 4$) was observed for phosphatidylcholines (PC) such as *m/z* 734.5 [PC (32:0)+H]$^+$, 760.5 [PC(34:1)+H]$^+$, and *m/z* 782.5 [PC(34:1)+Na]$^+$. The MS/MS identified lipid species are shown in Table 1 in the online Data Supplement. The calculated increase values and CVs for the selected ions are displayed in Supplemental Table 2. The addition of glycerol also increased the signal to noise ratio by a minimum of 3-fold.

Parameters such as time of spray, number of laser shots, and IPA/glycerol ratios (data not shown) were also evaluated

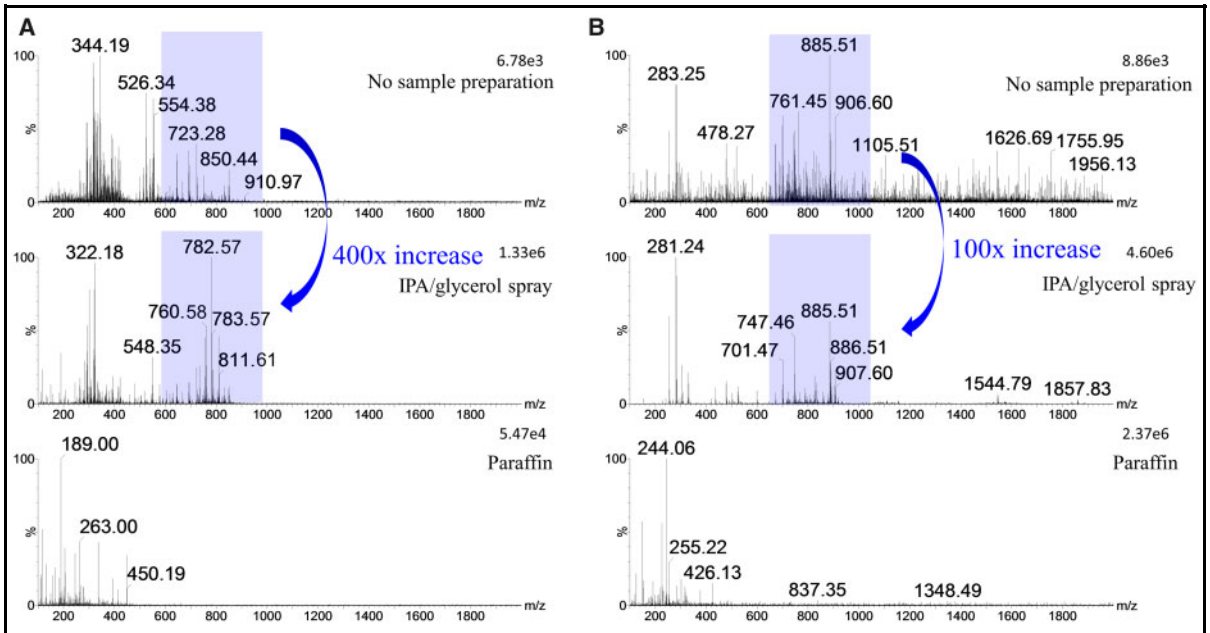

Fig. 1. Formalin-fixed paraffin-embedded brain tissue spectra. SpiderMass acquired (A), positive and (B), negative ion mode mass spectra of FFPE brain tissue sections. The top spectra were acquired without the sample preparation, the middle with the 2 passes of 50% isopropyl alcohol (IPA)/glycerol spray and the bottom spectra correspond to the paraffin. The highlighted (blue box) lipid mass range *m/z* 600–1000 indicates the signal intensity increase by 400x in positive and 100× in negative mode between the sample without the sample preparation and the sprayed slide.

Table 1. Cross-validation results. Cross-validation results of 4-class/2 -class dog sarcoma and 4-class/3-class human sarcoma models with model type, cross-validation type, *N* of classes, *N* spectra, *N* of passes as well as *N* of failures, *N* outliers, and percentage of correct classification accuracies after cross-validation.

							Correct classification accuracy (%)	
Model type	Cross-validation type	*N* classes	*N* spectra	*N* passes	*N* failures	*N* outliers	Excluding outliers	Including outliers
Canine sarcoma	5-fold	4	235	208	2	25	99.5	90.3
	One-patient-out	4	235	191	3	41	99.2	80.8
	5-fold	2	204	202	1	1	100	99.5
	One-patient-out	2	204	182	1	21	99.5	91.5.
Human sarcoma	5-fold	4	116	104	10	2	91.3	89.7
	One-patient-out	4	116	78	28	10	73.6	67.2
	5-fold	3	101	97	3	1	97.0	96.0
	"One-patient-out"	3	101	77	19	5	80.2	76.2

to produce maximum intensity mass spectrometry molecular profiles, minimal sample preparation time, and a homogeneous layer of matrix. The data are shown in Supplemental Figs 1–3. The tests revealed that 10 s and 20% glycerol/IPA were sufficient to obtain a homogeneous layer, reproducible and high intensity signals (up to $10e^5$). To reinforce the importance of analyzing nondewaxed FFPE samples, we investigated the influence of tissue dewaxing on the detected species, which revealed only 10 residual fatty acids remaining (Supplemental Fig. 4).

EVALUATING WALDI–MS ANALYTICAL PERFORMANCES FROM FFPE CLINICAL SAMPLES

The lipidomic screening of FFPE tissues was operated in a two-stage workflow (Fig. 2). First (Fig. 2, A), following the optimized sample preparation protocol, a molecular database using histologically annotated samples and molecular data was constructed through machine learning algorithms (training). Second, these classification models were used to perform interrogation of blind samples within <5 min (Fig. 2, B) (test).

The first FFPE classification databank was generated by analyzing a cohort (29 patients; 76 samples; 235 spectra) of canine veterinary sarcoma patients. The collected FFPE blocks followed 4 main sarcoma classes from diverse breeds and tumor origin (Supplemental Table 3). We investigated whether the lipido-molecular profiles could discriminate between the subtypes. The results are shown in Supplemental Fig. 5. The PCA plot of 4 canine sarcoma types is described with PC1 41.7%, PC2 21.6%, and PC 3 10.3% variance. The selected PCAs were subjected to supervised LDA analysis according to 4 subtypes (Supplemental Fig. 5, C). A substantial discrimination was observed in LD1 from leiomyosarcoma compared to the remaining subtypes; however, they were also separating from each other in LD2 and LD3. The model gave 99.5% cross-validation accuracy using 5-fold and 99.2% cross-validation accuracy using leave-one-patient out (Table 1). Since some of the subtypes were under-represented, we reconstructed the model including only angiosarcoma and leyiomyosarcoma (Supplemental Fig. 5, B and D). In this case, the cross-validation accuracy was improved to 100% using 5-fold and 99.5% using leave-one-patient out (Table 1).

HISTOLOGICAL CLASSIFICATION OF FFPE HUMAN SARCOMA TISSUES

A conceptual databank was created using a cohort of human sarcoma FFPE samples (29 patients, 37 samples, 116 spectra). Sarcomas were classified based on different subtypes and classes (malignant and benign) from optical images (Fig. 3, A). The samples were collected from

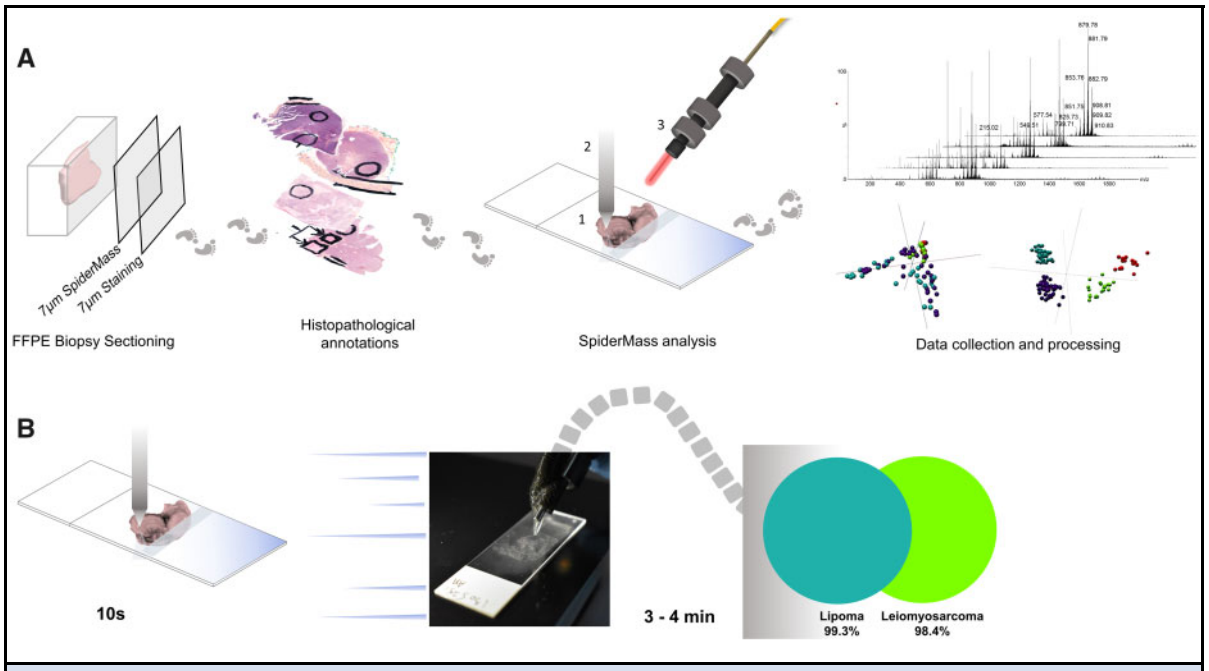

Fig. 2. A schematic workflow of the formalin-fixed paraffin-embedded (FFPE) screening experiment. (A), Steps to build the molecular database. The FFPE blocks are consecutively sectioned onto slides for SpiderMass analysis and hematoxylin-phloxine-saffron staining. The first section is hematoxylin-phloxine-saffron stained and annotated by the trained pathologist. The tissue heterogeneity is usually expressed as healthy, necrotic, or cancer region. Following the annotation, the consecutive slide is sprayed with the 20% glycerol/isopropyl alcohol solution and analyzed by the SpiderMass. Each region is measured separately and the data is recorded as mass spectra. The data files are imported into Abstract Model Builder software and subjected to principal component analysis-linear discriminant analysis based on their type and heterogeneity. (B), Blind tissue screening (5 min). The fast screening of a blind sample interrogates the database and provides classification based on the type and tissue heterogeneity. In the case of FFPE sarcoma the sections are classified either as lipoma, liposarcoma, leiomyoma, or leiomyosarcoma.

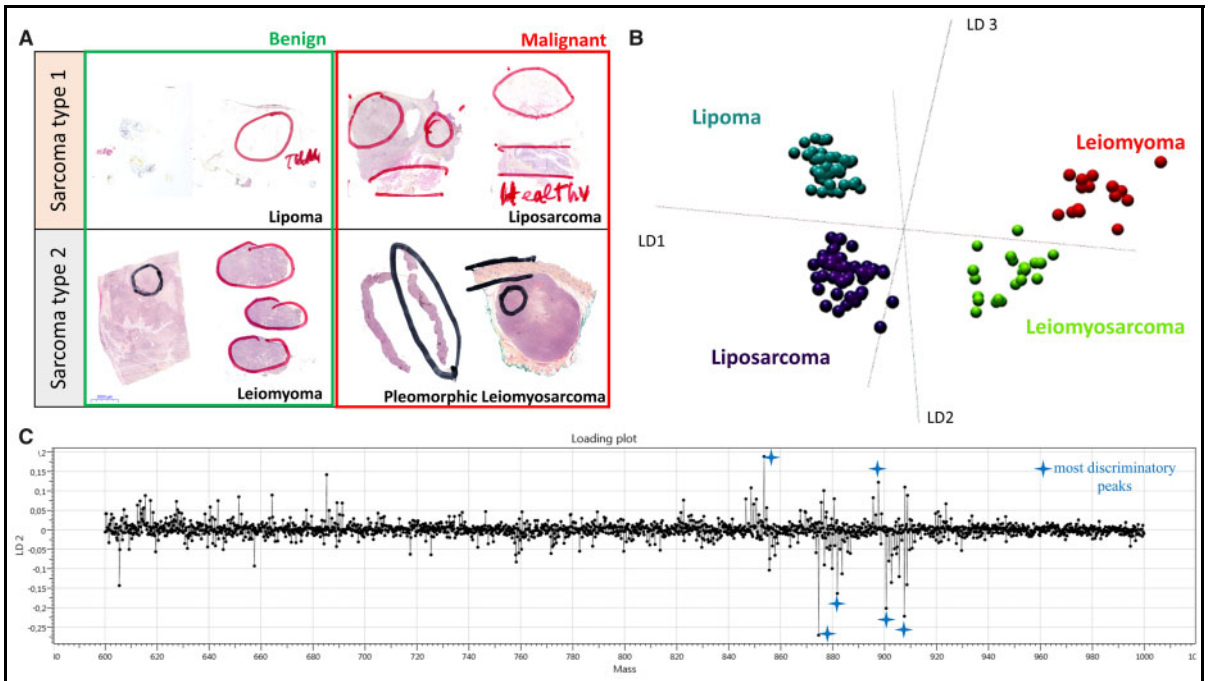

Fig. 3. Building the principal component analysis-linear discriminant analysis (PCA-LDA) classification model based on 4 human sarcoma types (lipoma, liposarcoma, eiomyoma, or leiomyosarcoma). (A), Examples of histopathological stains and annotations of formalin-fixed paraffin-embedded sarcoma samples. The table separates them based on their type (sarcoma type 1:lipoma, liposarcoma and sarcoma type 2: leiomyoma and leiomyosarcoma) and based on tumor classification: benign (green box) or malignant (red box). (B), LDA representation of the 4-class PCA-LDA. The LD1 discriminates between the 2 sarcoma types. The model was built from the individual spectra recorded in positive ion mode. (C), LD1 loading plot showing the discrimination between the benign (green) and malignant (red) tumors. The blue stars indicate the most discriminatory peaks: *m/z* 855.8, 879.8, 881.8, 897.8, 900.8, and 907.8.

patients with different ages, sexes, and tumors (Supplemental Table 4). The acquired spectra for each subtype are shown in Supplemental Fig. 6. The first 3 PCs explained >80% of the total variance in the dataset (Supplemental Fig. 7) due to intra- and interpatient heterogeneity, particularly for lipoma and liposarcoma, which had a considerable number of subtypes and tumor origin (Supplemental Table 4). The supervised LDA analysis is represented by the 3D plot in Fig. 3, B. The first component clearly discriminated between the 2 sarcoma types (LD 1), while the second discriminated between the lipoma and liposarcoma cancer types (LD 2). LD3 discriminated between leiomyoma and leiomyosarcoma. The loadings plot of LD2 is shown in Fig. 3, C. The LD2 loadings spectra showed the most discriminatory lipid peaks (blue stars). MS/MS analysis identified the selected molecular species (Supplemental Table 5 and Supplemental Fig. 8). Lipids contributing the most to the discrimination corresponded to a mixture of triglycerides (TG). The model gave cross-validation accuracies 91.2% using 5-fold and 73.8% using the leave-one-patient out method (Table 1). However, if we removed the under-represented leiomyoma and reconstructed the 3-class model again, the cross-validation accuracies improved to 97.0% using 5-fold and 80.2% using the leave-one-patient out method. In both models, 9 benign spectra were misclassified to their malignant counterpart and vice versa.

BLIND SCREENING OF FFPE SAMPLES

The quality of the human sarcoma classification model was evaluated by blind tissue analysis. Two sarcoma subtypes were randomly selected. Each mass spectrometry acquisition was automatically compared to the classification model in AMX software and resulted in a readout of different color codes and percentages of certainty of correspondence to one of the subtypes included in the classification model: leiomyoma (red), leiomyosarcoma (green), lipoma (turquoise), and liposarcoma (purple). The results of the 2 blind acquisitions are shown in Supplemental Videos 1 and 2. In the first case, the software predicted the sample to be a benign lipoma with >98.3% certainty for all 3

acquisitions. In the second case, the software predicted the sample to be a benign leiomyoma (red) with >95.4% certainty for all 3 scans. The histological annotations confirmed the correct classification in both cases.

EFFECT OF FFPE CONSERVATION TIME ON MOLECULAR PROFILES

We investigated the cutoff for the year of FFPE embedding and their consequences on molecular profiles. A human lipoma sample embedded in 2019 was analyzed before and after sample preparation (Fig. 4, A and B). There was an increase in absolute intensities, reaching $10e^4$ following the 20% glycerol/IPA spray. For comparison, an untreated fresh-frozen human lipoma sample is shown in Fig. 4, C. While lipid peaks between m/z 800–950 were retained in FFPE tissue, several lipids (PCs and phosphatidylethanolamines) in the mass range *m/z* 700–800 were depleted. The identity of the *m/z* 881.8 species was confirmed in both tissues by MS/MS analysis (Supplemental Fig. 9). We also performed an age dependence study, reprocessing the spectra from leiomyosarcoma samples ($n = 8$, 20 spectra) at different years of embedding (2014–2019). The results are shown in Fig. 5. A drop in intensity from $1e^4$ to $1e^3$ was observed in the *m/z* 600–900 between the years 2014 and 2019 (Fig. 5, A and Supplemental Fig 10). The PCA analysis further depicted the impact of conservation time. The PC 1 showed a 62.3% variance (Fig. 5, B); The loading-mass plot of PC1 (data not shown) indicated 4 most significant diglycerides (DG) and triglyceride (TG) peaks *m/z* 643.6 DG (36:2)/DG (38:5)Na^+, *m/z* 853.8 TG (52:5)/TG(50:2) Na^+, *m/z* 879.8 TG (54:6)/TG(52:3)Na^+, and *m/z* 881.8 TG (54:5)/TG(52:2)Na^+ to contribute to the variance. Additional statistical tests (Fig. 5, C) showed a significant difference in signal intensities for *m/z* 853.8 ($P = 0.0059$), 879.8 ($P = 0.0069$). and 881.8 ($P = 0.0126$) between the samples embedded in 2016 and 2019 and only *m/z* 881.8 between 2015 and 2019 ($P = 0.0466$). No significant difference ($P > 0.05$) was observed between the years 2014 and 2019. However, we can observe a loss of absolute intensities ($n = 5$) when analyzing leiomyosarcoma samples embedded after a period.

Discussion

Here we report the direct lipid profiling of FFPE tissues with WALDI–MS for potential postoperative clinical translation. Because the method does not require deparaffinization and rehydration, which has been confirmed to alter lipid profiles (18, 21, 22), but only a fast spray (deposition of glycerol matrix, ≤1 min), neither costly equipment nor well trained staff are necessary to operate the platform. By introducing a glycerol mixture to promote desorption/ionization mainly in positive ion mode, we have shown the possibility of obtaining histologically different lipidomic features and using them to classify clinical samples of different origin (canine, human) and fixation protocols. This rapid analysis (<5 min) meets the requirements of the clinical turnaround time while analyzing >100 samples per day.

For our proof-of-concept, we developed canine and human sarcoma lipido-histological databanks. Sarcomas are a rare and complex type of cancer and can, for canines and humans, form over 100 different heterogeneous mesenchymal lesions (29). Current diagnostic methods include standard histological staining, immunostaining, and molecular genetics (30, 31). However, without the new ancillary testing methods, the first-hand morphological diagnostic approach can be extremely challenging particularly for tumors of intermediate malignant potential (32–34). Interestingly, soft tissue tumor subtypes known to be difficult to distinguish morphologically by the pathologist (lipoma versus well-differentiated liposarcoma or liposarcoma lipoma-like) (35) were distinguished by the molecular fingerprints. The most abundant triglycerides, TG (52:4)/TG(50:1)Na^+, TG (54:5)/TG(52:2)Na^+, and TG (56:6)/TG(54:3)Na^+, found discriminant in benign lipomas, have also been previously shown to decrease in fresh-frozen high-grade myxoid liposarcomas (36).

Although PCA analysis reflected on tumor heterogeneity associated to the origin of the tumors, the databanks gave 99.1% cross-validation accuracy using 5-fold and 98.5% cross-validation accuracy using leave-one-patient out and 91.2% cross-validation accuracy using 5-fold and 73.8% cross-validation accuracy using leave-one-patient out for canine and human sarcoma subtyping, respectively. Although the leaving-one-patient-out (24, 37) method is the reference cross-validation technique, it also produces errors when dealing with under-represented classes. This is well exemplified for subtypes with lower clinical occurrence. Once the model was rebuilt for only 3 subtypes, the cross-validation improved. Nevertheless, the interrogation of 2 blind samples resulted in correct classification accuracy above 95% for leiomyoma and above 98% for lipoma (Fig. 5). To improve the model robustness, additional samples and independent data are needed to robustly test the performance of the model.

We also investigated the effects of FFPE conservation time on the lipid profiles. Crosslinking continues to progress and the older the block the tighter are the crosslinked networks. Differences can be observed by loss of less abundant proteins in old samples (38) as well as degradation of certain classes of lipid species on FF (39). Recently, high-performance LC–MS was performed on archived hospital samples and lipid standards to investigate lipid profiles after FF (15). Phospholipids (PLs) were shown to undergo hydrolysis or modifications (N-methylation and N-formylation

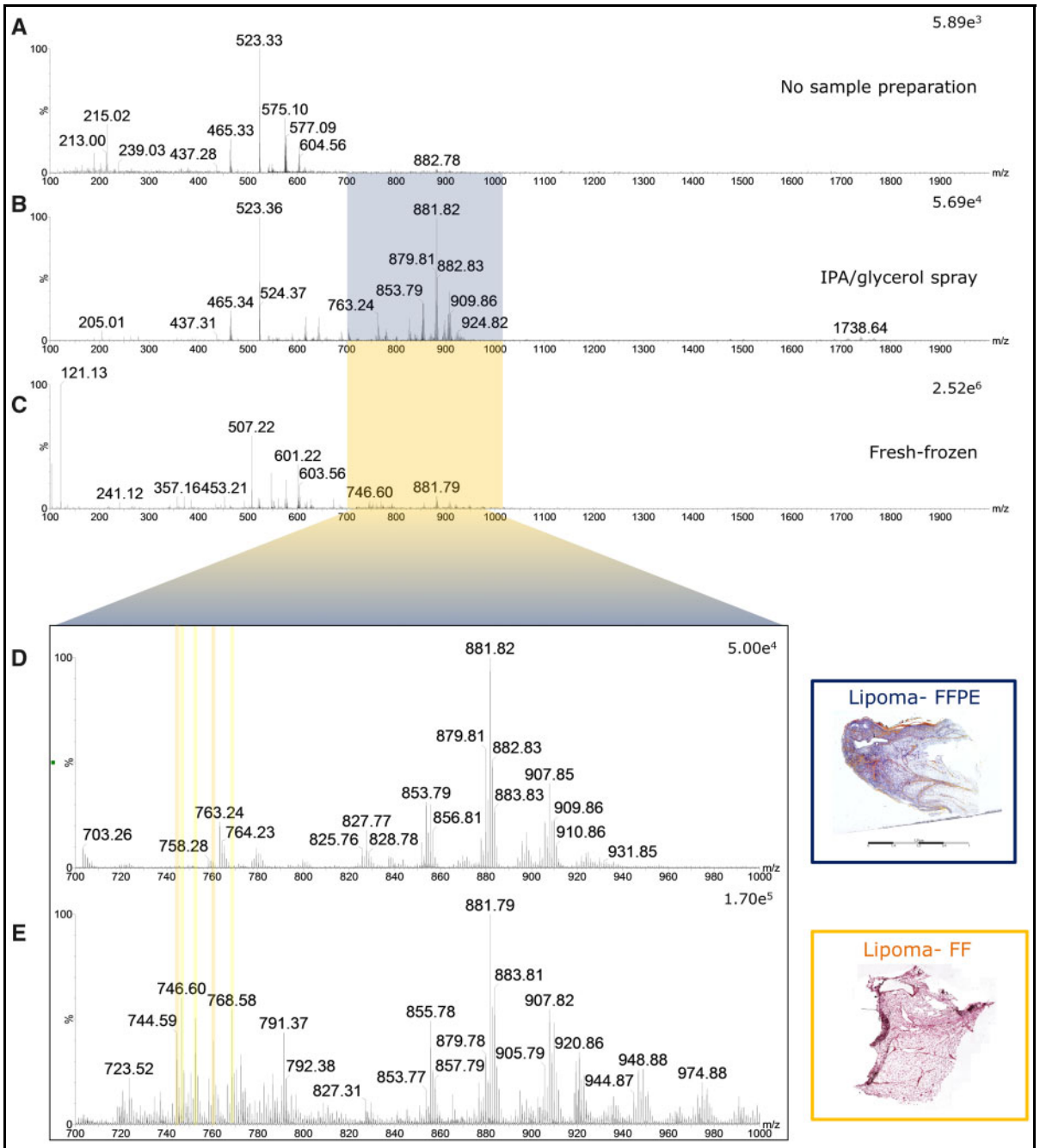

Fig. 4. Acquired spectra of the formalin-fixed paraffin-embedded (FFPE) and fresh-frozen (FF) lipoma tissue in positive ion mode. The FFPE tissue sections of lipoma (A), without sample preparation and with (B), 10 s glycerol/isopropyl alcohol (IPA) spray. FFPE lipoma molecular profile was compared with (C), fresh-frozen lipoma molecular profile without sample preparation. (D) and (E) correspond to zoom in the *m/z* region (700–1000) of mass spectra presented in (C) and (D), respectively, as well as hematoxylin-phloxine-saffron stained optical scans of the analyzed tissue sections. The yellow bars indicate the depleted phosphatidylcholines and phosphatidylethanolamine species in FFPE sarcoma compared to fresh-frozen tissue.

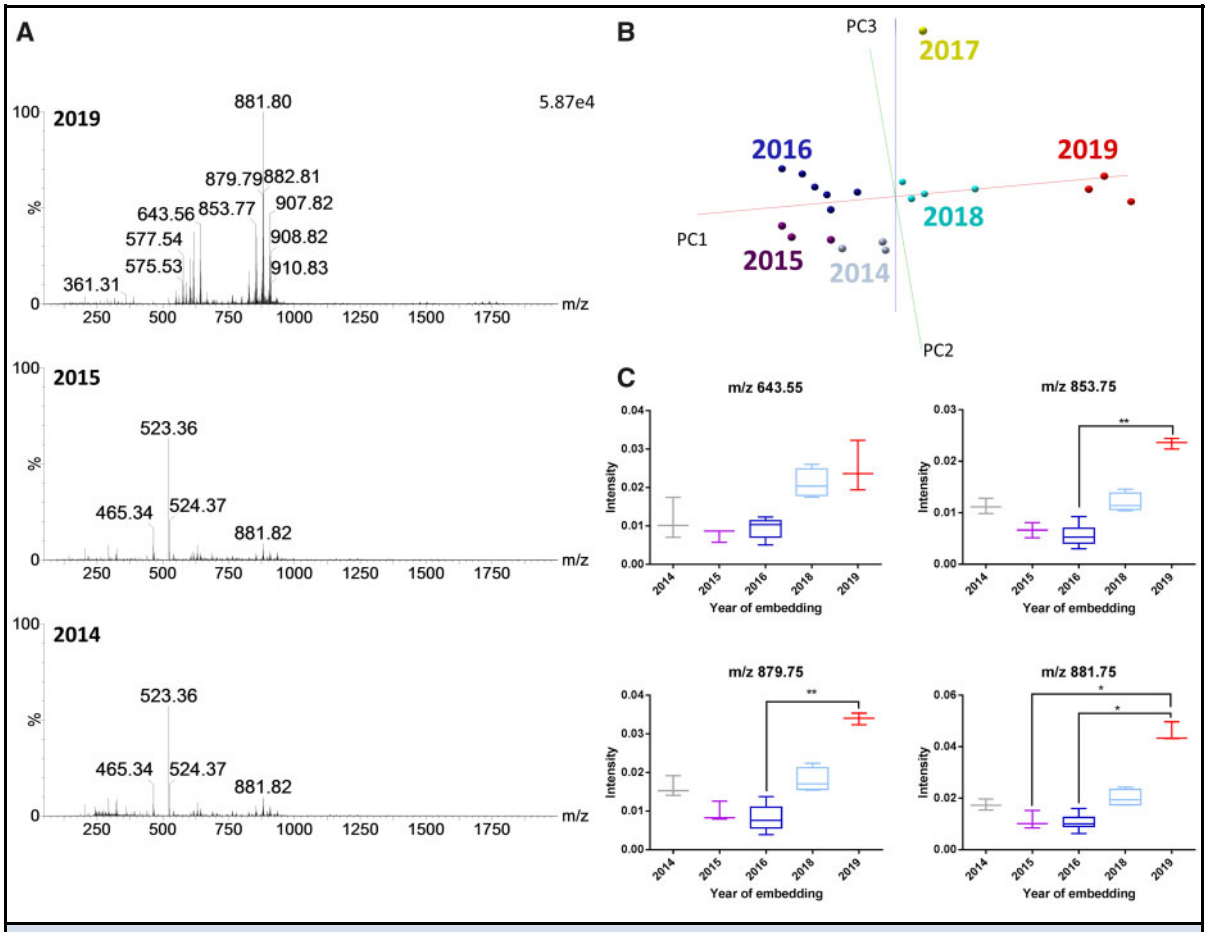

Fig. 5. Effects of conservation on the mass spectra acquired from leiomyosarcoma samples. (A), SpiderMass representation spectra (of 10 laser shots) acquired from the samples preserved since 2014, 2015, and 2016. The spectra have been scaled to $5.87e^4$ intensity. There was an intensity drop in the mass range between 600–1000 *m/z* for the years 2014 and 2015 compared to 2019. (B), Six-class principal component analysis visualization model built from different time points of leiomyosarcoma samples (from 2014 to 2019). The PC 1 describes 62.27% variance; PC 2 describes 12.47% and PC 3 11.29%. There is a very clear separation by PC 1 between the 2019 and bundle at 2014, 2015, and 2016. (C), Relative intensity boxplots of the selected peaks showing the highest contribution to the variance of PC1. The intensities were normalized to the total ion chromatogram and represented as boxplots for each year with Tukey method whisker definition. There was a significant difference for *m/z* 853.76 (**$P = 0.0059$), *m/z* 879.75(**$P = 0.0069$), *m/z* 881.75 (*$P = 0.0126$) between the year 2016 and 2019 and *m/z* 881.75 (*$P = 0.0466$) between the year 2015 and 2019.

for phospholipids bearing an amine) while the sphingolipids remained unmodified. PL concentrations were also found decreased by MALDI–MS in FF rat brain tissues (40) and in FF mouse kidney (16). We also observed similar effects in our study. While PLs in rat brain remained unchanged, a drop in absolute lipid signal intensity was observed when comparing fresh-frozen to FFPE lipoma tissue. Particularly, PE signals are depleted in FFPE lipoma, in line with these species being crosslinked by the primary amine group. However, the rate of lipid crosslinking has never been quantified. TGs showed no observable difference. Hydrolysis of PLs was also observed in our data as previously reported (15). However, hydrolysis is not expected to increase with the conservation time. Thus, we hypothesize the decrease of intensities arises from the increase of crosslinking in the older samples. However, no time dependent study was previously performed from FFPE tissues to systematically investigate the effect of conservation time. In our study, despite the decrease of certain lipid signals, statistical tests indicated that only 3 ions show a significant difference.

To conclude, by demonstrating the analysis of non-dewaxed FFPE samples, we have laid the groundwork

for the creation of a rapid WALDI–MS platform to screen and classify sarcoma tissues. The sarcoma databanks are just one of the examples where the platform could be used for consolidation of histopathological diagnosis. Tissue banks with different types of cancer FFPE tissue could use this platform. However, implementation into the clinics will require further expansion of the database and analysis of different FFPE clinical tissues, as well as on-site validation of larger sample cohorts. Moreover, we determined that human sarcoma samples up to 6 years of age could be used to create the databank. Future automation would provide a new, fast, and robust tool to help with patient stratification.

Supplemental Material

Supplemental material is available at *Clinical Chemistry* online.

Nonstandard Abbreviations: FFPE, formalin-fixed paraffin-embedded; FF, formalin fixed; WALDI–MS, water-assisted laser desorption ionization mass spectrometry.

Ethics approval and consent to participate: All experiments were approved by the local Ethics Committee (CPP Nord Ouest IV 12/10) in accordance with the French and European legislation. Prior to the experiments, patients signed an informed consent and authorization form describing the experimental protocol. No personal information was used in these experiments, and a random number was assigned to each sample.

Consent for Publication: All patient consent was obtained for publication.

Availability of Data and Material: All raw data have been deposited to the Mendeley Data repository and will be accessible with a code prior to publication.

Author Contributions: *All authors confirmed they have contributed to the intellectual content of this paper and have met the following 4 requirements: (a) significant contributions to the conception and design, acquisition of data, or analysis and interpretation of data; (b) drafting or revising the article for intellectual content; (c) final approval of the published article; and (d) agreement to be accountable for all aspects of the article thus ensuring that questions related to the accuracy or integrity of any part of the article are appropriately investigated and resolved.*

I. Fournier and N. Ogrinc wrote the manuscript original draft; N. Ogrinc and I. Fournier designed the experiments; N. Ogrinc, P.-D. Caux, and B. Fatou performed the experiments. E. Bouchaert and D. Tierny collected the canine sarcoma samples and performed the histology. Y.-M. Robin and D. Bertin collected the human sarcoma samples, performed histology and validated diagnostics. I. Fournier, N. Ogrinc, P.-D. Caux, and B. Fatou analyzed the data. I. Fournier, M. Salzet, Y.-M. Robin, and Z. Takats corrected the manuscript. I. Fournier and M. Salzet supervised the project, and M. Ziskind, C. Focsa, M. Salzet, and I. Fournier provided the funding.

Authors' Disclosures or Potential Conflicts of Interest: *Upon manuscript submission, all authors completed the author disclosure form. Disclosures and/or potential conflicts of interest:*

Employment or Leadership: E. Bouchaert is an employee of OCR. D. Tierny is founder and CEO of OCR. Z. Takats, Imperial College London.
Consultant or Advisory Role: Z. Takats, Waters Corporation.
Stock Ownership: None declared.
Honoraria: None declared.
Research Funding: This work was funded by Ministère de l'Enseignement Supérieur, de la Recherche et de l'Innovation, Université de Lille and Inserm. The project was also funded by Institut Universitaire de France (I. Fournier) and Région Hauts de France-EU FEDER O'DREAMS (D. Tierny, I. Fournier, M. Salzet). ISite ULNE, Region Haut de France-EU FEDER and OCR funded the PhD of P.-D. Caux.
Expert Testimony: None declared.
Patents: M. Ziskind, C. Focsa, M. Salzet, and I. Fournier are inventors on a patent (priority number WO2015IB57301 20150922) related to part of the described protocol. The system is under protection by patent CA2961491 A1 (29). B. Fatou, FR3026189; M. Ziskind, WO2016046748(A1); I. Fournier, WO2016046748A1.

Role of Sponsor: The funding organizations played no role in the design of study, choice of enrolled patients, review and interpretation of data, preparation of manuscript, or final approval of manuscript.

Acknowledgments: We wish to thank Marc Le Parquier from the "Centre d'Études et de Recherches, Lasers et Applications" (CERLA) of the University of Lille for his technical support.

REFERENCES

1. Joseph S, Janakiraman R, Chacko G, Jayaraj R, Thomas M, Thomas M, et al. Predictability of recurrence using immunohistochemistry to delineate surgical margins in mucosal head and neck squamous cell carcinoma (PRISM-HNSCC): study protocol for a prospective, observational and bilateral study in Australia and India. BMJ Open 2017;7:e014824.
2. Mino-Kenudson M, Chirieac LR, Law K, Hornick JL, Lindeman N, Mark EJ, et al. A novel, highly sensitive antibody allows for the routine detection of ALK-rearranged lung adenocarcinomas by standard immunohistochemistry. Clin Cancer Res 2010;16:1561–71.
3. Longuespée R, Casadonte R, Kriegsmann M, Pottier C, Muller GD, Delvenne P, et al. MALDI mass spectrometry imaging: a cutting-edge tool for fundamental and clinical histopathology. Proteomics Clin Appl 2016;10:701–19.
4. Quanico J, Franck J, Wisztorski M, Salzet M, Fournier I. Progress and potential of imaging mass spectrometry applied to biomarker discovery. In: FH Kobeissy, StevensJr, M Stanley, editors. Neuroproteomics: methods and protocols. New York (NY): Springer; 2017. p. 21–43.
5. DeHoog RJ, Zhang J, Alore E, Lin JQ, Yu W, Woody S, et al. Preoperative metabolic classification of thyroid nodules using mass spectrometry imaging of fine-needle aspiration biopsies. Proc Natl Acad Sci USA 2019;116:21401–8.
6. Puchtler H, Meloan SN. On the chemistry of formaldehyde fixation and its effects on immunohistochemical reactions. Histochemistry 1985;82:201–4.
7. Lemaire R, Desmons A, Tabet JC, Day R, Salzet M, Fournier I. Direct analysis and MALDI imaging of formalin-fixed, paraffin-embedded tissue sections. J Proteome Res 2007;6:1295–305.
8. Wisztorski M, Franck J, Salzet M, Fournier I. Mass spectrometry imaging: principles and protocols. In: SS Rubakhin, JV Sweedler, editors. MALDI direct analysis and imaging of frozen versus FFPE tissues: what strategy for which sample? Totowa (NJ): Humana Press; 2010. p. 303–22.
9. Judd AM, Gutierrez DB, Moore JL, Patterson NH, Yang J, Romer CE, et al. A recommended and verified procedure for in situ tryptic digestion of formalin-fixed paraffin-embedded tissues for analysis by matrix-assisted laser desorption/ionization imaging mass spectrometry. J Mass Spectrom 2019;54:716–27.
10. Coscia F, Doll S, Bech JM, Schweizer L, Mund A, Lengyel E, et al. A streamlined mass spectrometry–based

proteomics workflow for large-scale FFPE tissue analysis. J Pathol 2020;251:100–12.
11. Powers TW, Neely BA, Shao Y, Tang H, Troyer DA, Mehta AS, et al. MALDI imaging mass spectrometry profiling of N-glycans in formalin-fixed paraffin embedded clinical tissue blocks and tissue microarrays. PLoS ONE 2014;9: e106255.
12. Han X. Lipidomics for studying metabolism. Nat Rev Endocrinol 2016;12:668–79.
13. Sulciner ML, Gartung A, Gilligan MM, Serhan CN, Panigrahy D. Targeting lipid mediators in cancer biology. Cancer Metastasis Rev 2018;37:557–72.
14. Touboul D, Brunelle A, Laprévote O. Mass spectrometry imaging: towards a lipid microscope? Biochimie 2011; 93:113–9.
15. Gaudin M, Panchal M, Ayciriex S, Werner E, Brunelle A, Touboul D, et al. Ultra performance liquid chromatography–mass spectrometry studies of formalin-induced alterations of human brain lipidome. J Mass Spectrom 2014;49:1035–42.
16. Vos DRN, Bowman AP, Heeren RMA, Balluff B, Ellis SR. Class-specific depletion of lipid ion signals in tissues upon formalin fixation. Int J Mass Spectrom 2019;446: 116212.
17. Buck A, Heijs B, Beine B, Schepers J, Cassese A, Heeren RMA, et al. Round robin study of formalin-fixed paraffin-embedded tissues in mass spectrometry imaging. Anal Bioanal Chem 2018;410:5969–80.
18. Ly A, Buck A, Balluff B, Sun N, Gorzolka K, Feuchtinger A, et al. High-mass-resolution MALDI mass spectrometry imaging of metabolites from formalin-fixed paraffin-embedded tissue. Nat Protoc 2016;11:1428–43.
19. Hughes C, Gaunt L, Brown M, Clarke NW, Gardner P. Assessment of paraffin removal from prostate FFPE sections using transmission mode FTIR-FPA imaging. Anal. Methods 2014;6:1028–35.
20. Pietrowska M, Gawin M, Polańska J, Widłak P. Tissue fixed with formalin and processed without paraffin embedding is suitable for imaging of both peptides and lipids by MALDI-MS. Proteomics 2016;16: 1670–7.
21. Kelly AD, Breitkopf SB, Yuan M, Goldsmith J, Spentzos D, Asara JM. Metabolomic profiling from formalin-fixed, paraffin-embedded tumor tissue using targeted LC/MS/MS: application in sarcoma. PLoS One 2011;6:e25357.
22. Cacciatore S, Zadra G, Bango C, Penney KL, Tyekucheva S, Yanes O, et al. Metabolic profiling in formalin-fixed and paraffin-embedded prostate cancer tissues. Mol Cancer Res 2017;15:439–47.
23. Fatou B, Saudemont P, Leblanc E, Vinatier D, Mesdag V, Wisztorski M, et al. In vivo real-time mass spectrometry for guided surgery application. Sci Rep 2016;6:25919.
24. Ogrinc N, Saudemont P, Balog J, Robin Y-M, Gimeno J-P, Pascal Q, et al. Water-assisted laser desorption/ionization mass spectrometry for minimally invasive in vivo and real-time surface analysis using SpiderMass. Nat Protoc 2019;14:3162–82.
25. Saudemont P, Quanico J, Robin Y-M, Baud A, Balog J, Fatou B, et al. Real-time molecular diagnosis of tumors using water-assisted laser desorption/ionization mass spectrometry technology. Cancer Cell 2018;34: 840–851. e4.
26. Sud M, Fahy E, Cotter D, Brown A, Dennis EA, Glass CK, et al. LMSD: LIPID MAPS structure database. Nucleic Acids Res 2007;35:D527–32.
27. Smith CA, O'Maille G, Want EJ, Qin C, Trauger SA, Brandon TR, et al. METLIN: a metabolite mass spectral database. Ther Drug Monit 2005;27:747-51.
28. Overberg A, Karas M, Bahr U, Kaufmann R, Hillenkamp F. Matrix-assisted infrared-laser (2.94 μm) desorption/ionization mass spectrometry of large biomolecules. Rapid Commun Mass Spectrom 1990;4:293–6.
29. Bleloch JS, Ballim RD, Kimani S, Parkes J, Panieri E, Willmer T, et al. Managing sarcoma: where have we come from and where are we going? Ther Adv Med Oncol 2017;9:637–59.
30. Antonescu CR. The role of genetic testing in soft tissue sarcoma. Histopathology 2006;48:13–21.
31. Jaber OI, Kirby PA. Alveolar soft part sarcoma. Arch Pathol Lab Med 2015;139:1459–62.
32. Mentzel T, Palmedo G, Kuhnen C. Well-differentiated spindle cell liposarcoma ('atypical spindle cell lipomatous tumor') does not belong to the spectrum of atypical lipomatous tumor but has a close relationship to spindle cell lipoma: clinicopathologic, immunohistochemical, and molecular analysis of six cases. Mod Pathol 2010; 23:729–36.
33. Deyrup A, Chibon F, Guillou L, Lagarde P, Coindre J-M, Weiss S. Fibrosarcoma-like lipomatous neoplasm: a reappraisal of so-called spindle cell liposarcoma defining a unique lipomatous tumor unrelated to other liposarcomas. Am J Surg Pathol 2013;37:1373–8.
34. World Health Organization. WHO Classification of Tumours of Soft Tissue and Bone. 4th Ed. WHO, OMS, 2020. https://apps.who.int/bookorders/anglais/detart1.jsp?codlan=1&codcol=70&codcch=4005 (Accessed March 2020).
35. Azzopardi JG, Iocco J, Salm R. Pleomorphic lipoma: a tumour simulating liposarcoma. Histopathology 1983;7: 511–23.
36. Willems SM, van Remoortere A, van Zeijl R, Deelder AM, McDonnell LA, Hogendoorn PC. Imaging mass spectrometry of myxoid sarcomas identifies proteins and lipids specific to tumour type and grade, and reveals biochemical intratumour heterogeneity. J Pathol 2010; 222:400–9.
37. Balog J, Sasi-Szabó L, Kinross J, Lewis MR, Muirhead LJ, Veselkov K, et al. Intraoperative tissue identification using rapid evaporative ionization mass spectrometry. Sci Transl Med 2013;5:194ra93.
38. Donczo B, Guttman A. Biomedical analysis of formalin-fixed, paraffin-embedded tissue samples: the Holy Grail for molecular diagnostics. J Pharm Biomed Anal 2018; 155:125–34.
39. Deierkauf FA, Heslinga FJM. The action of formaldehyde on rat brain lipids. J Histochem Cytochem 1962;10: 79–82.
40. Carter CL, McLeod CW, Bunch J. Imaging of phospholipids in formalin fixed rat brain sections by matrix assisted laser desorption/ionization mass spectrometry. J Am Soc Mass Spectrom 2011;22:1991–8.